

Magnetic confinement of massless Dirac fermions in graphene

A. De Martino, L. Dell'Anna, and R. Egger

Institut für Theoretische Physik, Heinrich-Heine-Universität, D-40225 Düsseldorf, Germany

(Dated: February 4, 2008)

Due to Klein tunneling, electrostatic potentials are unable to confine Dirac electrons. We show that it is possible to confine massless Dirac fermions in a monolayer graphene sheet by inhomogeneous magnetic fields. This allows one to design mesoscopic structures in graphene by magnetic barriers, e.g. quantum dots or quantum point contacts.

PACS numbers: 73.21.-b, 73.63.-b, 75.70.Ak

The successful preparation of monolayer graphene films [1, 2, 3] has recently generated a lot of excitement and allows one to directly probe the physics of two-dimensional (2D) Dirac-Weyl fermions. The massless Dirac spectrum at low energy scales is caused by the sublattice structure (the basis of graphene's honeycomb lattice contains two carbon atoms, giving rise to an isospin degree of freedom) combined with a special band structure, and has been verified experimentally [1, 2, 4]. Besides the fundamental interest, graphene has also been suggested as a building block for future nanoelectronic devices [3]. However, there is an interesting twist at that point, since Dirac fermions cannot immediately be confined by electrostatic potentials. In marked contrast to the Schrödinger case, Dirac fermions can penetrate high and wide electrostatic barriers with high transmission probability, in particular for normal incidence. This is often referred to as *Klein tunneling* [5] and can be understood by noting that under the barrier, the whole spectrum is shifted upwards. Incoming electron-like quasiparticles can then efficiently tunnel through the barrier via empty states in the hole band, which are always available since the Dirac spectrum is unbounded. In the context of carbon nanotubes and graphene, this effect was theoretically studied in Refs. [6, 7, 8]. The creation of useful mesoscopic structures, e.g. quantum dots or quantum point contacts, thus seems to encounter a major and fundamental obstacle, seriously limiting graphene's potential for applications.

An obvious but rather crude way out of this dilemma is to mechanically cut samples into the desired shape. Alternatively, one could attempt to exploit the fact that suitable transverse states in a graphene strip may allow one to circumvent Klein tunneling [9]. Here we describe a completely different and hitherto unnoticed way of confining Dirac-Weyl quasiparticles in graphene by *magnetic barriers*. Employing existing technology, the required *inhomogeneous* static magnetic field configurations can be created using ferromagnetic layers located beneath the substrate on which the graphene layer is deposited; for other possibilities, see Ref. [10]. Mesoscopic transport with magnetic barriers has been experimentally studied for the Schrödinger fermions realized in conventional semiconductor heterostructures, e.g. transport in the presence of magnetic barriers [11] and superlattices [12], magnetic edge states close to a magnetic step [13],

and magnetically confined quantum dots or antidots [14]. Correspondingly, apart from one study of magnetic edge states in narrow-gap semiconductors [15], model calculations have only been carried out for Schrödinger fermions [10, 16, 17, 18]. Here we formulate the theory of magnetic barriers and magnetic quantum dots for the massless Dirac-Weyl fermions in graphene. With minor modifications, the theory also covers narrow-gap semiconductors.

We focus on a static *orbital* magnetic field [19] oriented perpendicular to the graphene ($x-y$) plane, $\mathbf{B} = B(x, y)\hat{e}_z$, and work on the simplest possible theory level (no disorder, no interactions), where the electronic spin degree of freedom can be disregarded. Moreover, we consider the physically relevant case of slow $B(x, y)$ variations on the scale of the graphene lattice spacing ($a = 0.246$ nm). On low energy scales, a weakly doped (or undoped) graphene layer is described by two identical copies of the Dirac Hamiltonian, which remain decoupled in the presence of smoothly varying magnetic fields [20]. These two copies describe low-energy envelope states in the $\mathbf{k} \cdot \mathbf{p}$ approach [21] close to the two relevant K points in the hexagonal first Brillouin zone of graphene. For slowly varying $\mathbf{B} = \text{rot } \mathbf{A}$, we therefore need to study just one K point. The time-independent Dirac equation for the spinor $\psi(x, y) = (\psi_+, \psi_-)^T$ at energy $E = v_F \epsilon$ then reads (we put $\hbar = 1$)

$$\vec{\sigma} \cdot \left(\mathbf{p} + \frac{e}{c} \mathbf{A}(x, y) \right) \psi(x, y) = \epsilon \psi(x, y), \quad (1)$$

where the Fermi velocity is $v_F \approx 8 \times 10^5$ m/sec, the momentum operator is $\mathbf{p} = -i(\partial_x, \partial_y)^T$, and the 2×2 Pauli matrices in $\vec{\sigma} = (\sigma_x, \sigma_y)$ act in isospin space. The velocity operator follows from the Heisenberg equation as $\mathbf{v} = v_F \vec{\sigma}$. In this paper, we discuss two prime examples of interest based on the Dirac-Weyl Hamiltonian in Eq. (1), namely, (i) the magnetic barrier and (ii) a circularly symmetric magnetic quantum dot.

For a *magnetic barrier*, the relevant physics is described by a magnetic field translationally invariant along the (say) y -direction, $B(x, y) = B(x)$. Choosing the vector potential in the gauge $\mathbf{A}(x, y) = A(x)\hat{e}_y$ with $\partial_x A(x) = B(x)$, transverse momentum p_y is conserved, and for given p_y , Eq. (1) leads to the coupled equations

$$[\partial_x \pm p_y \pm (e/c)A(x)]\psi_{\pm}(x) = i\epsilon\psi_{\mp}(x). \quad (2)$$

These equations imply the decoupled 1D 'Schrödinger' equations

$$[\partial_x^2 - V_{\pm}(x) + \epsilon^2]\psi_{\pm}(x) = 0, \quad (3)$$

with the p_y -dependent effective potentials

$$V_{\pm}(x) = \pm(e/c)\partial_x A(x) + [p_y + (e/c)A(x)]^2. \quad (4)$$

Let us then describe the solution of Eq. (3) for a *square-well magnetic barrier*, where $\mathbf{B} = B_0\hat{e}_z$ (with constant B_0) within the strip $-d \leq x \leq d$ but $\mathbf{B} = 0$ otherwise,

$$B(x, y) = B_0 \theta(d^2 - x^2), \quad (5)$$

with the Heaviside step function θ . The sharp-edge form (5) is appropriate when the Fermi wavelength λ_F is parametrically larger than the edge smearing length λ_s , while $\lambda_s \gg a$ to ensure smoothness of \mathbf{B} ; otherwise scattering between the two K points takes place [23]. Note that here $\lambda_F \sim 1/|\epsilon|$ is determined by the (inverse) Fermi momentum of the Dirac quasiparticles, which is measured relative to the relevant K point, and the large momentum scale associated with the K point itself drops out completely. With the magnetic length $l_B \equiv \sqrt{c/eB_0}$, the vector potential is written as

$$A(x) = \frac{c}{\epsilon l_B^2} \times \begin{cases} -d, & x < -d \\ x, & |x| \leq d \\ d, & x > d \end{cases}. \quad (6)$$

Consider now an electron-like scattering state ($\epsilon > 0$) entering from the left side, with incoming momentum $\mathbf{p} = (p_x, p_y)$. The incoming wave function is, up to an overall normalization,

$$\psi_{in}(x) = \left(\frac{1}{\frac{p_x + i(p_y - d/l_B^2)}{|\mathbf{p}|}} \right) e^{ip_x x},$$

where the shift in p_y is due to our gauge choice for the vector potential. It is then convenient to parametrize the momenta as

$$p_x = \epsilon \cos \phi, \quad p_y = \epsilon \sin \phi + d/l_B^2. \quad (7)$$

The gauge-invariant velocity is $\mathbf{v} = v_F(\cos \phi, \sin \phi)^T$, and therefore ϕ is the kinematic incidence angle. The emergence angle ϕ' at the right barrier, $p'_x = \epsilon \cos \phi'$, is obtained by exploiting conservation of p_y ,

$$\sin \phi' = \frac{2d}{\epsilon l_B^2} + \sin \phi. \quad (8)$$

Up to an overall normalization factor, the scattering state in the three regions is as follows. For $x < -d$,

$$\psi_I(x) = \begin{pmatrix} 1 \\ e^{i\phi} \end{pmatrix} e^{ip_x x} + r \begin{pmatrix} 1 \\ -e^{-i\phi} \end{pmatrix} e^{-ip_x x} \quad (9)$$

with ϕ -dependent reflection amplitude r . In the barrier region $|x| \leq d$, the solution is expressed in terms of parabolic cylinder functions D_ν [24],

$$\psi_{II} = \sum_{\pm} c_{\pm} \begin{pmatrix} D_{(\epsilon l_B)^2/2-1}(\pm\sqrt{2}(x/l_B + p_y l_B)) \\ \pm i \frac{\sqrt{2}}{\epsilon l_B} D_{(\epsilon l_B)^2/2}(\pm\sqrt{2}(x/l_B + p_y l_B)) \end{pmatrix} \quad (10)$$

with complex coefficients c_{\pm} . Finally, for $x > d$, the transmitted wave is

$$\psi_{III}(x) = t \sqrt{p_x/p'_x} \begin{pmatrix} 1 \\ e^{i\phi'} \end{pmatrix} e^{ip'_x x} \quad (11)$$

with transmission amplitude t . The transmission probability $T = |t|^2$ is then related to the reflection probability $R = |r|^2$ by $T + R = 1$. Note that Eq. (8) implies that for certain incidence angles ϕ , no transmission is possible. In fact, under the condition

$$\epsilon l_B \leq d/l_B, \quad (12)$$

every incoming state is *reflected*, regardless of the incidence angle ϕ . In essence, all states with cyclotron radius (defined under the magnetic barrier) less than d will bend and exit backwards again. This illustrates our main finding: in contrast to electrostatic barriers, *magnetic barriers are able to confine Dirac-Weyl quasiparticles*. For sufficiently large barrier width $2d$ and/or field B_0 , all relevant states will be reflected. Our analysis also shows that this conclusion is generic and does not depend on the particular choice (5) for the barrier.

If the condition (12) is not obeyed, the transmission probability T does not vanish in general. Its value follows by enforcing continuity of the wavefunction at $x = \pm d$. The solution of the resulting linear algebra problem yields the transmission amplitude in closed form,

$$t = \frac{2i\epsilon l_B \sqrt{2p'_x/p_x} \cos \phi}{e^{i(p_x + p'_x)d} \mathcal{D}} (u_2^+ v_2^- + v_2^+ u_2^-), \quad (13)$$

$$\begin{aligned} \mathcal{D} &= (\epsilon l_B)^2 e^{i(\phi' - \phi)} (u_1^+ u_2^- - u_2^+ u_1^-) \\ &\quad - 2(v_1^+ v_2^- - v_2^+ v_1^-) + i\sqrt{2}\epsilon l_B \\ &\quad \times \left(e^{i\phi'} (v_1^+ u_2^- + u_2^+ v_1^-) + e^{-i\phi} (u_1^+ v_2^- + v_2^+ u_1^-) \right), \end{aligned}$$

where we use the shorthand notation

$$\begin{aligned} u_1^{\pm} &\equiv D_{(\epsilon l_B)^2/2-1}(\pm\sqrt{2}(-d/l_B + p_y l_B)), \\ v_1^{\pm} &\equiv D_{(\epsilon l_B)^2/2}(\pm\sqrt{2}(-d/l_B + p_y l_B)). \end{aligned}$$

The related symbols u_2^{\pm}, v_2^{\pm} follow by letting $-d \rightarrow d$. The resulting transmission probability $T(\phi) = |t|^2$ is shown in Figure 1 for several parameter values (ϵ, d) outside the perfectly reflecting regime specified in Eq. (12). For a typical value of $B_0 = 4$ T, the magnetic length is $l_B = 13$ nm, and $\epsilon l_B = 1$ corresponds to $E = 44$ meV. Standard fabrication and doping techniques should thus be sufficient to enter the perfect reflection regime. On the

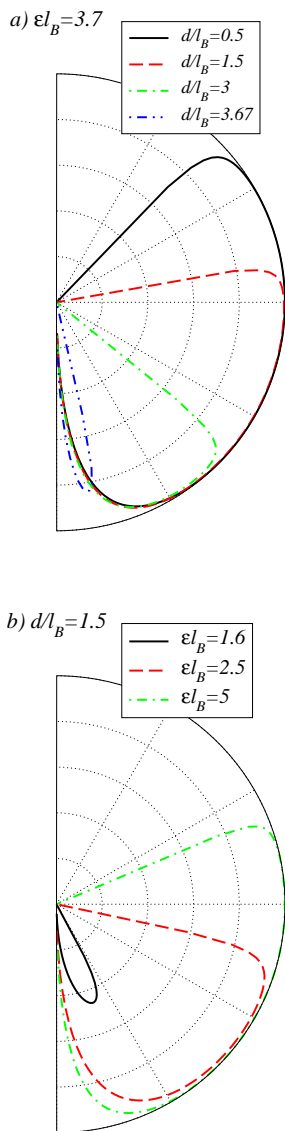


FIG. 1: (Color online) Polar graphs depicting the transmission probability $T(\phi)$ for a magnetic barrier of width $2d$ at various energies ϵ . The outermost semicircle corresponds to $T = 1$, the center to $T = 0$, with grid spacing 0.2. Angles between $-\pi/2$ and $+\pi/2$ are shown, the angular grid spacing is $\pi/6$. (a) T as function of barrier width for fixed energy, $\epsilon l_B = 3.7$. For $d/l_B \geq 3.7$, the transmission is zero for all ϕ . (b) Same as function of ϵ for $d/l_B = 1.5$. The transmission vanishes for $\epsilon l_B \leq 1.5$.

other hand, for sufficiently high energy and/or narrow barriers, the ϕ -dependent transmission profile in Fig. 1 should be observable.

We now turn to a discussion of a circularly symmetric *magnetic quantum dot*, defined by a radially inhomogeneous field $\mathbf{B} = B(r)\hat{e}_z$. It is convenient to use complex variables $z = x + iy$ (not to be confused with the z -direction) and $\bar{z} = x - iy$, and the corresponding derivatives $\partial = \frac{1}{2}(\partial_x - i\partial_y)$ and $\bar{\partial} = \frac{1}{2}(\partial_x + i\partial_y)$, where $r = \sqrt{\bar{z}z}$. Writing in a similar manner $A = A_x + iA_y$ and

$\bar{A} = A_x - iA_y$, the magnetic field is $B(r) = -i(\partial A - \bar{\partial}\bar{A})$, where $(e/c)A = i\varphi(r)/\bar{z}$ and $(e/c)\bar{A} = -i\varphi(r)/z$. This gauge expresses the vector potential in terms of the magnetic flux $\varphi(r)$ through a disc of radius r in units of the flux quantum hc/e ,

$$\varphi(r) = \frac{e}{c} \int_0^r dr' r' B(r'). \quad (14)$$

Next, we recall that in 2D the group of rotations is $SO(2) \sim U(1)$, whose generator is the orbital angular momentum operator $L = z\partial - \bar{z}\bar{\partial}$, with eigenfunctions $\sim z^m$ (integer m). For an isotropic field $B(r)$, the operator $J = L + \sigma_z/2$ is conserved, i.e. eigenstates of Eq. (1) are classified by the half-integer eigenvalue $j = m \pm 1/2$ of J ,

$$\begin{pmatrix} \psi_+ \\ \psi_- \end{pmatrix} = \frac{1}{\sqrt{2\pi}} \begin{pmatrix} \phi_m(r)(z/r)^m \\ \chi_m(r)(z/r)^{m+1} \end{pmatrix}. \quad (15)$$

The Dirac equation (1) then reduces to a pair of radial 1D equations for $\phi_m(r)$ and $\chi_m(r)$ (where $r > 0$ and $f' = df/dr$),

$$\begin{aligned} \phi'_m - \frac{m + \varphi(r)}{r} \phi_m &= i\epsilon \chi_m, \\ \chi'_m + \frac{m + 1 + \varphi(r)}{r} \chi_m &= i\epsilon \phi_m, \end{aligned} \quad (16)$$

implying a second-order equation for the upper component of Eq. (15),

$$\phi''_m + \frac{1}{r} \phi'_m + \left(\epsilon^2 - \frac{e}{c} B(r) - \frac{(m + \varphi(r))^2}{r^2} \right) \phi_m = 0, \quad (17)$$

plus a similar equation for $\chi_m(r)$. For $\epsilon \neq 0$, χ_m directly follows from ϕ_m via Eq. (16).

We now analyze a simple model for a magnetic quantum dot, where $B = B_0$ outside a disk of radius R and zero inside, as previously considered for Schrödinger fermions in Ref. [22]. The flux (14) is with $l_B = \sqrt{c/eB_0}$ given by

$$\varphi(r) = \frac{r^2 - R^2}{2l_B^2} \theta(r - R). \quad (18)$$

With normalization constant \mathcal{N}_m and $m \leq 0$, the states

$$\psi_m^{\epsilon=0} = \mathcal{N}_m \left(\frac{r}{R} \right)^{\theta(r-R)R^2/2l_B^2} e^{-\varphi(r)/2} \begin{pmatrix} 0 \\ (z/r^2)^m \end{pmatrix}$$

represent zero-energy solutions of Eq. (1). The remaining eigenspectrum comes in pairs $\pm\epsilon$, and we focus on the $\epsilon > 0$ sector. Up to an overall normalization factor, Eq. (17) implies Bessel function solutions inside the dot, $\phi_m^< = J_m(\epsilon r)$ for $r < R$. The general solution $\phi_m^>$ outside the dot ($r > R$) involves the degenerate hypergeometric functions Φ and Ψ [24]. With $\xi = r^2/2l_B^2$ and $\tilde{m} = m - \delta$, where $\delta = R^2/2l_B^2$ is the missing flux through the dot, we obtain

$$\phi_m^> = \xi^{|\tilde{m}|/2} e^{-\xi/2} (a_1 \Phi(\alpha, 1 + |\tilde{m}|; \xi) + a_2 \Psi(\alpha, 1 + |\tilde{m}|; \xi)). \quad (19)$$

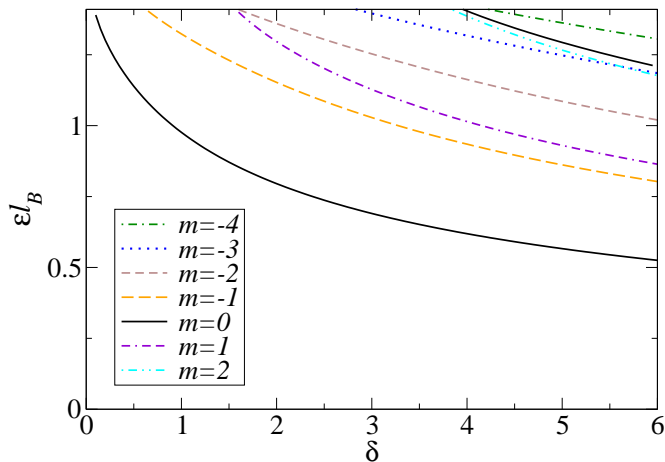


FIG. 2: (Color online) Low-energy eigenenergies (labeled by m) for a disk-like magnetic quantum dot in graphene versus missing flux $\delta = R^2/2l_B^2$.

Here $a_{1,2}$ are arbitrary complex coefficients, and energy is parameterized by

$$\alpha = 1 + \tilde{m}\theta(\tilde{m}) - (\epsilon l_B)^2/2. \quad (20)$$

Continuity of $\psi(r)$ at $r = R$ now implies continuity of both $\phi_m(r)$ and $\phi'_m(r)$, see Eq. (16). The resulting two matching conditions then determine the possible eigenstates.

Note that the well-known relativistic Landau levels (for $R = 0$) correspond to $\alpha = -n$ (with $n = 0, 1, 2, \dots$) [20], where Φ and Ψ reduce to Laguerre polynomials. For

finite R , the matching problem does *not* admit solutions with $\alpha = -n$, and we thus consider $\alpha \neq -n$. However, for $\alpha \neq -n$, Φ has the asymptotic behavior $\Phi \sim e^\xi$ at $\xi \rightarrow \infty$, i.e. normalizability of ψ necessarily requires $a_1 = 0$ in Eq. (19). One of the two conditions then fixes a_2 , and the other determines the quantization condition on the energy,

$$1 - |\tilde{m}|\theta(-\tilde{m})/\delta - \frac{\epsilon l_B}{\sqrt{2\delta}} \frac{J_{m+1}(\epsilon l_B \sqrt{2\delta})}{J_m(\epsilon l_B \sqrt{2\delta})} \quad (21)$$

$$= \frac{d}{d\xi} \ln \Psi(\alpha, 1 + |\tilde{m}|; \xi = \delta).$$

The numerical solution of Eq. (21) is possible using standard root finding methods (bracketing and bisection). In Figure 2, we show the solutions to Eq. (21) with $\epsilon > 0$ but below the lowest positive-energy bulk Landau level located at $\epsilon l_B = \sqrt{2}$. Within the shown δ range, for $m \neq 0$, there is at most one solution with $0 < \epsilon l_B < \sqrt{2}$, while for $m = 0$, we obtain two such solutions for $\delta \gtrsim 4$. Depending on the missing flux $\delta \sim R^2 B_0$, the energy levels of this 'Dirac dot' can be tuned almost at will.

To conclude, we have described a new way of confining Dirac-Weyl quasiparticles in graphene. We hope that our work will guide experimental efforts to the development of mesoscopic structures based on this novel material, and stimulate more theoretical work on the effects of magnetic barriers on Dirac fermions.

We thank A. Altland, T. Heinzl, and W. Häusler for discussions. This work was supported by the SFB TR 12 of the DFG and by the ESF network INSTANS.

-
- [1] K.S. Novoselov *et al.*, *Science* **306**, 666 (2004); *Nature* **438**, 197 (2005).
 - [2] Y. Zhang, Y.W. Tan, H. Stormer, and P. Kim, *Nature* **438**, 201 (2005).
 - [3] C. Berger *et al.*, *Science* **312**, 1191 (2006).
 - [4] S.Y. Zhou *et al.*, *Nature Physics* **2**, 595 (2006).
 - [5] For a pedagogical review, see A. Calogeracos and N. Dombey, *Contemporary Physics* **40**, 313 (1999).
 - [6] T. Ando, T. Nakanishi, and R. Saito, *J. Phys. Soc. Jpn.* **67**, 2857 (1998).
 - [7] V.V. Cheianov and V.I. Falko, *Phys. Rev. B* **74**, 041403 (2006).
 - [8] M.I. Katsnelson, K.S. Novoselov, and A.K. Geim, *Nature Physics* **2**, 620 (2006).
 - [9] P.G. Silvestrov and K.B. Efetov, cond-mat/0606620.
 - [10] S.J. Lee, S. Souma, G. Ihm, and K.J. Chang, *Phys. Rep.* **394**, 1 (2004).
 - [11] M. Johnson, B.R. Bennett, M.J. Yang, M.M. Miller, and B.V. Shanabrook, *Appl. Phys. Lett.* **71**, 974 (1997); V. Kubrack *et al.*, *J. Appl. Phys.* **87**, 5986 (2000).
 - [12] H.A. Carmona *et al.*, *Phys. Rev. Lett.* **74**, 3009 (1995); P.D. Ye *et al.*, *ibid.* **74**, 3013 (1995).
 - [13] A. Nogaret, S.J. Bending, and M. Henini, *Phys. Rev. Lett.* **84**, 2231 (2000).
 - [14] K.S. Novoselov, A.K. Geim, S.V. Dubonos, Y.G. Cornelissens, F.M. Peeters, and J.C. Maan, *Phys. Rev. B* **65**, 233312 (2002).
 - [15] N. Malkova, I. Gómez, and F. Domínguez-Adame, *Phys. Rev. B* **63**, 035317 (2001).
 - [16] F.M. Peeters and A. Matulis, *Phys. Rev. B* **48**, 15166 (1993).
 - [17] A. Matulis, F.M. Peeters, and P. Vasilopoulos, *Phys. Rev. Lett.* **72**, 1518 (1994).
 - [18] I.S. Ibrahim and F.M. Peeters, *Phys. Rev. B* **52**, 17321 (1995).
 - [19] The Zeeman field can easily be included but does not affect our conclusions.
 - [20] G.W. Semenoff, *Phys. Rev. Lett.* **53**, 2449 (1984).
 - [21] D.P. DiVincenzo and E.J. Mele, *Phys. Rev. B* **29**, 1685 (1984).
 - [22] J. Reijniers, F.M. Peeters, and A. Matulis, *Phys. Rev. B* **59**, 2817 (1999).
 - [23] The limit $B_0 \rightarrow \infty$ cannot be taken without spoiling consistency of the single-valley approach.
 - [24] I.S. Gradshteyn and I.M. Ryzhik, *Table of Integrals, Series, and Product* (Academic Press, Inc., 1980).